ESRF	**Experiment title:** Tungstate scheelites at high pressures. Part II: $SrWO_4$	**Experiment number**: HS2120
Beamline: ID09A	**Date of experiment**: from: 4/4/03 to: 8/4/03	**Date of report**: 30/5/05
Shifts: 12	**Local contact(s)**: M. Hanfland	*Received at ESRF:*

Names and affiliations of applicants:

Andrzej Grzechnik (1), Wilson A. Crichton (2)

(1) Universidad del País Vasco, Bilbao

(2) ESRF

Report:

At ambient conditions, strontium tungstate $SrWO_4$ has the scheelite $CaWO_4$ structure ($I4_1/a$, Z = 4) with the Sr^{2+} and W^{6+} cations eightfold and fourfold coordinated by oxygens, respectively. Recently, Christofilos et al. [1] have reported a reversible pressure-induced phase transition in $SrWO_4$ starting at 11.5 GPa as observed with Raman scattering. Several Raman bands have a non-linear behavior in the pressure range 11.5-15 GPa, that can be due to either a stabilization of the high-pressure polymorph or a formation of an additional (intermediate) phase. The crystal structure of the modification above 15 GPa, with distorted WO_4^{2-} tetrahedra, is supposedly related to the scheelite type. In the synchrotron angle-dispersive x-ray powder diffraction study on $CaWO_4$, the archetype for all the $MeWO_4$ (Me: Ca, Sr, Ba, Pb) compounds [2], it has been found that calcium tungstate ($I4_1/a$, Z = 4) transforms to the fergusonite structure (I2/a, Z = 4), a distorted variant of the scheelite type, above about 10 GPa at room temperature. Both scheelite ($I4_1/a$, Z = 4) and fergusonite (I2/a, Z = 4) structures are ordered superstructures of the fluorite type ($Fm\bar{3}m$, Z = 4) and there is no discontinuity in the pressure dependence of the unit cell volumes during the $I4_1/a \rightarrow I2/a$ transformation. Christofilos et al. [3] have earlier demonstrated that the low-energy Raman active modes in calcium tungstate exhibit softening during this phase transition. It is still not clear whether the scheelite $\rightarrow$ fergusonite structural change in $CaWO_4$

is of the first or second order. On the other hand, the temperature-induced $I4_1/a \rightarrow I2/a$ transformation in rare earth niobates and tantalates at atmospheric conditions is ferroelastic and associated with the anisotropic phonon softening of a transverse acoustic mode at the Brillouin zone center [4].

In this study, we investigate the pressure-induced phase transitions in $SrWO_4$ scheelite at room temperature as observed with synchrotron angle-dispersive x-ray powder diffraction in diamond anvil cells.

A sample of polycrystalline $SrWO_4$ scheelite (99.9+%, Chempur Feinchemikalien und Forschungsbedarf GmbH, Karlsruhe) has been finely ground in ethanol and loaded into a diamond anvil cell with a mixture of methanol and ethanol as a pressure transmitting medium, already used for Raman scattering experiments [1]. Angle-dispersive powder x-ray diffraction patterns have been measured at room temperature on the ID09a beamline. Monochromatic radiation at 0.41325 Å has been used for pattern collection on image plates. The images have been integrated using the program FIT2D [5] to yield intensity versus 2θ diagrams. The ruby luminescence method [6] has been used for pressure measurements.

X-ray powder patterns of $SrWO_4$ collected upon compression to 20.7 GPa are shown in Figures 1 and 2. Up to 8.8 GPa, the stable structure is of the scheelite type ($I4_1/a$, Z = 4). At higher pressures between 10.7 and 14.2 GPa, new weak reflections occur (Figure 2) that can fully be accounted for with the fergusonite type (I2/a, Z = 4) already observed for $CaWO_4$ above 10 GPa [2]. Several additional new x-ray peaks are detectable in the pressure range 15-20.7 GPa. They correspond neither to the fergusonite type nor to the $PbWO_4$-III ($P2_1/n$, Z = 8), $LaTaO_4$ ($P2_1/c$, Z = 4), $HgWO_4$ (C2/c, Z = 4), or $BaMnF_4$ ($Cmc2_1$, Z = 4) types previously considered as candidates for the pressure-induced post-scheelite structures [2,7]. Moreover, the patterns collected between 15 and 20.7 GPa cannot be indexed on a basis of a single $SrWO_4$ phase. The pressure-induced transformations are irreversible as several “non-scheelite” reflections are observed at atmospheric conditions. In fact, some of them are due to the WO_3 and SrO impurities that (upon close inspection of Figures 1 and 3) seem to be occurring upon compression above 15 GPa. It suggests that $SrWO_4$ tends to decompose above 15 GPa.

A Rietveld refinement of the pattern for $SrWO_4$ collected at 10.7 GPa has been carried out with the structural model of the $CaWO_4$ fergusonite (I2/a, Z = 4) [2] using the program JANA2000 [8] (Figure 4 and Table 1). The refined parameters have included the lattice parameters, fractional atomic coordinates, isotropic thermal parameters for the Sr and W atoms, overall intensity scaling factor, zero shift, GP and LX parameters for the pseudo-Voigt profile function. The isotropic thermal parameters O atoms have been fixed at 0.015 and not refined. The agreement factors are: R_p = 0.0347, wR_p = 0.0511, GoF = 0.9, R_{obs} = 0.0883, and wR_{obs} = 0.0639. The Sr atoms are eightfold coordinated to the oxygen atoms. The W-O bond lengths and the next-nearest-neighbour distances are 1.75-1.85 Å and 2.66-2.94 Å, respectively. Hence, the WO_4^{2-} tetrahedra are deformed but still isolated.

Figure 5 shows the pressure dependence of lattice parameters, unit-cell volumes, and c/a axial ratios for the scheelite ($I4_1/a$, Z = 4) and fergusonite (I2/a, Z = 4) polymorphs of $SrWO_4$ to 14.2 GPa extracted from the x-ray powder patterns (Figure 1) using the Le Bail method. The compression data including both phases of strontium tungstate cannot be fitted by a common Birch-Murnaghan equation of state. The unit-cell volumes at pressures up to 8.2 GPa are fitted with the zero-pressure bulk modulus B_0 = 66 ± 2 GPa, the first pressure derivative of the bulk modulus B' = 8.13 ± 5.1, and the unit-cell volume of scheelite at ambient pressure V_0 = 350.3 ± 1.74 $Å^3$. When B' is fixed at 4.0, the B_0 and V_0 parameters are 81 ± 4 GPa and 349.1 ± 1.0 $Å^3$, respectively. There is no significant volume collapse at the scheelite-fergusonite phase transition between 8.8 and 10.7 GPa. However, the fergusonite unit cells are less compressible than the scheelite ones. The c/a axial ratio is a measure of the tetragonal distortion of the fluorite superstructure, the ideal value being equal to 2. This ratio in scheelite as well as the b/a and b/c ratios in fergusonite decrease upon compression, indicating that $SrWO_4$ is more compressible along its unique crystallographic axis.

The results of our angle-dispersive x-ray powder diffraction investigations demonstrate that $SrWO_4$ scheelite ($I4_1/a$, Z = 4) transforms to fergusonite (I2/a, Z = 4) at about 10 GPa with the onset of decomposition above 15 GPa. The $I4_1/a \rightarrow I2/a$ transformation has already been observed not only in $CaWO_4$ [2] but also in $BaWO_4$ [9] and $CaMoO_4$ [10].

Our findings that SrWO4 decomposes at high pressures correspond to what has already been observed in several other materials. Silicate zircons ($ZrSiO_4$, $HfSiO_4$) and monazites, e.g., naturally dimorphous $ThSiO_4$ as thorite and huttonite [11], transform to scheelite structures and then, in some cases, decompose to component oxides under high-pressure conditions [12-14]. Similar behaviour is also evident from the work carried out on hydrothermally-prepared zircon and scheelite forms of $ZrGeO_4$ at high temperatures [15] and on fluoride scheelites [16].

References

1. D. Christofilos, K. Papagelis, S. Ves, G.A. Kourouklis, and C. Raptis, J. Phys.: Condens. Matter **14**, 12641 (2002).
2. A. Grzechnik, W.A. Crichton, M. Hanfland, and S. Van Smaalen, J.Phys.: Condens. Matter **15**, 7261 (2003).
3. D. Christofilos, S. Ves, and G.A. Kourouklis, phys. stat. sol. (b) **198**, 539 (1996).
4. S. Tsunekawa, T. Kamiyama, K. Sasaki, H. Asano, and F. Fukuda, Acta Cryst. A **49**, 595 (1993); S. Tsunekawa, T. Kamiyama, H. Asano, T. Fukuda, J. Solid State Chem. **116**, 28 (1995); S.V. Borisov and E.N. Ipatova, J. Struct. Chem. **35**, 865 (1994); I.A. Kondrateva, S.K. Filatov, L.V. Andrianova, and A.M. Korovkin, Inorg. Mater. **25**, 1446 (1989); K. Parlinski, Y. Hashi, S. Tsunekawa, and Y. Kawazoe, J. Mater. Res. **12**, 2428 (1997); Y. Kuroiwa, S. Aoyagi, T. Shobu, K. Nozawa, S. Tsunekawa, and Y. Noda, Jpn. J. Appl. Phys. **38**, 600 (1999).
5. A.P. Hammersley, S.O. Svensson, M. Hanfland, A.N. Fitch, and D. Häusermann, High Press. Res. **14**, 235 (1996).
6. G.J. Piermarini, S. Block, J.D. Barnett, and R.A. Forman, J. Appl. Phys. **46**, 2774 (1975); H.K. Mao, J. Xu, and P.M. Bell, J. Geophys. Res. **91**, 4673 (1986).
7. D. Errandonea, F.J. Manjón, M. Somayazulu, and D. Häusermann, J. Solid State Chem. **177** 1087 (2004).

8. V. Petricek, M. Dusek, and L. Palatinus, Jana2000. The crystallographic computing system. Institute of Physics, Praha, Czech Republic (2000): the weighing scheme $w = [\sigma^2(F_{obs})]^{-1}$, $w' = w/(4F_{obs}^2)$, GoF = $((\Sigma w(|F_{obs}|-|F_{calc}|)^2)/(m-n))^{1/2}$, $R_{obs} = (\Sigma||F_{obs}|-|F_{calc}||)/(\Sigma|F_{obs}|)$, $wR_{obs} = ((\Sigma w'(|F_{obs}|-|F_{calc}|)^2)/(\Sigma w'|F_{obs}|^2))^{1/2}$. F_{obs} and F_{calc} are the observed and calculated structure factors scaled one to the other, respectively. m is the number of reflections and n is the number of refined parameters

9. V. Panchal, N. Garg, A.K. Chauhan, B. Sangeeta, and S.M. Sharma, Solid State Commun. **130** 203 (2004).

10. W. Crichton, A. Grzechnik, Z. Kristall. NCS **219** (2004) 337 (2004).

11. M. Taylor and R.C. Ewing, R.C., Acta Cryst. B**34**, 1074 (1978).

12. L. Liu, Earth Planet. Sci. Lett. **44**, 390 (1979).

13. L. Liu, Earth Planet. Sci. Lett. **57**, 110–116 (1982).

14. S. Ono, Y. Tange, I. Katayama, and T. Kikegawa, Amer. Mineral. **89**, 185 (2004).

15. M. Hirano and H. Morikawa, Chem. Mater. **15**, 2561 (2003).

16. A. Grzechnik, W.A. Crichton, P. Bouvier, V. Dmitriev, H.-P. Weber, and J.-Y. Gesland, J. Phys.: Condens. Matter **16**, 7779 (2004); A. Grzechnik, K. Friese, V. Dmitriev, H.-P. Weber, J.-Y. Gesland, and W.A. Crichton, J. Phys.: Condens. Matter **17**, 763 (2005).

Table 1 Structural parameters of fergusonite $SrWO_4$ at 10.7 GPa: I2/a, a = 5.2494(5) Å, b = 11.3759(8) Å, c = 5.2756(4) Å, β = 90.16(1)°, V = 315.04(5) $Å^3$. Estimated standard deviations are in parentheses.

Atom	Site	x	y	z	U_{iso}
Sr	4e	¼	0.621(2)	0	0.014(1)
W	4e	¼	0.1223(7)	0	0.0160(6)
O1	8f	0.943(9)	0.962(5)	0.202(8)	0.015
O2	8f	0.498(9)	0.220(4)	0.868(9)	0.015

Selected distances (Å)

Sr_O1	2.60(5)	(2x)
	2.44(5)	(2x)
Sr_O2	2.61(5)	(2x)
	2.25(5)	(2x)
W_O1	1.75(5)	(2x)
	2.66(5)	(2x)
W_O2	1.85(5)	(2x)
	2.94(5)	(2x)

Figure Captions

Figure 1 Selected x-ray powder patterns of $SrWO_4$ upon compression.

Figure 2 Selected x-ray powder patterns of $SrWO_4$ upon compression in the 2θ region from 3.8° to 4.5°. The dashed line shows the pressure shift of the (020) reflection in the fergusonite structure (I2/a, Z = 4).

Figure 3 X-ray powder patterns of $SrWO_4$ upon decompression.

Figure 4 Observed, calculated, and difference x-ray powder patterns for fergusonite $SrWO_4$ at 10.7 GPa (λ = 0.41325 Å) - I2/a, a = 5.2494(5) Å, b = 11.3759(8) Å, c = 5.2756(4) Å, β = 90.16(1)°, V = 315.04(5) $Å^3$. Vertical markers indicate Bragg reflections.

Figure 5 Pressure dependence of lattice parameters of $SrWO_4$. Full and open symbols represent the parameters for the scheelite ($I4_1/a$, Z = 4) and fergusonite (I2/a, Z = 4) polymorphs, respectively.

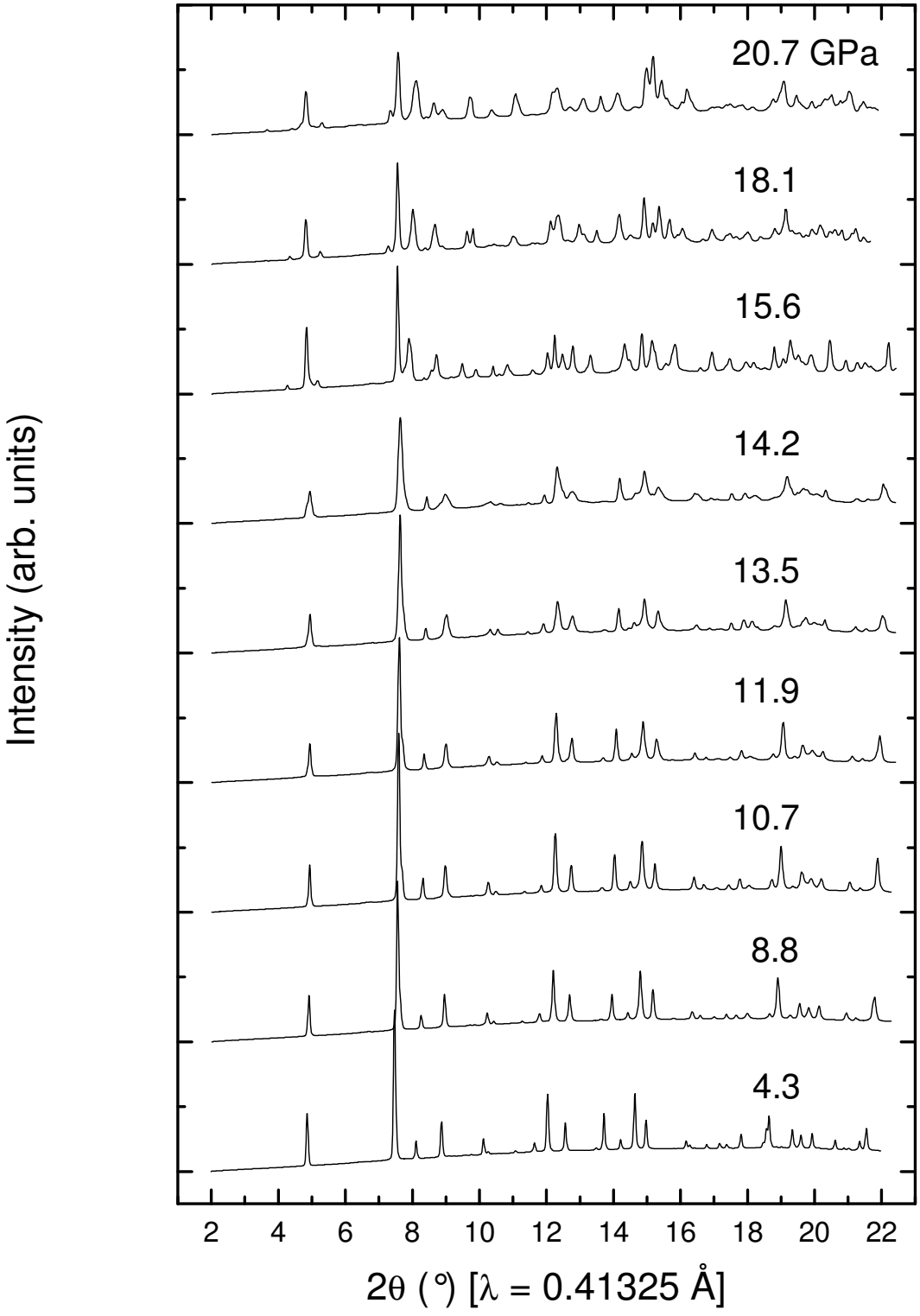
20.7 GPa
18.1
15.6
14.2
13.5
11.9
10.7
8.8
4.3
Intensity (arb. units)
2
4
6
8
10
12
14
16
18
20
22
2θ (°) [λ = 0.41325 Å]

Figure 1.

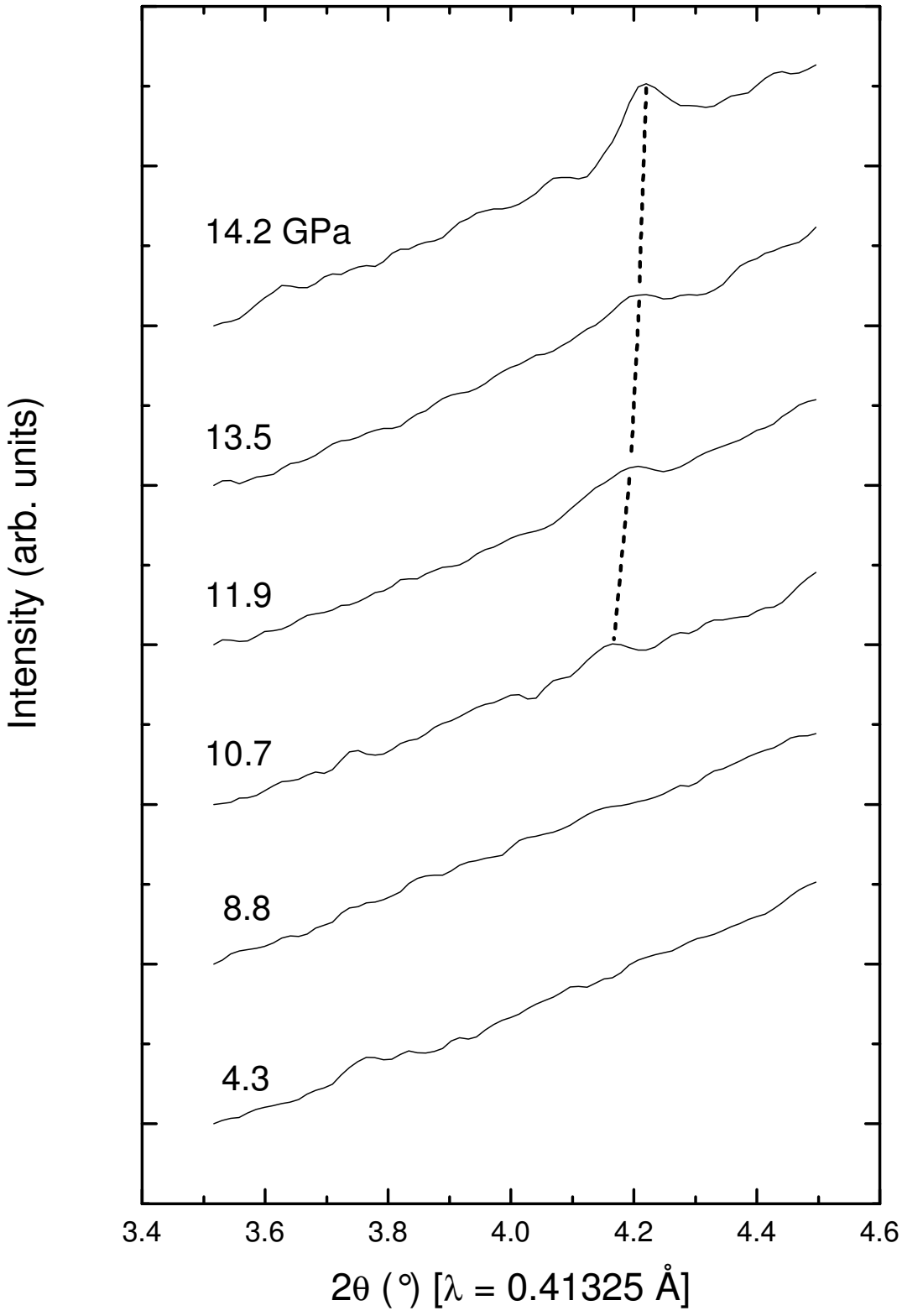
14.2 GPa
13.5
11.9
10.7
8.8
4.3
Intensity (arb. units)
3.4
3.6
3.8
4.0
4.2
4.4
4.6
2θ (°) [λ = 0.41325 Å]

Figure 2.

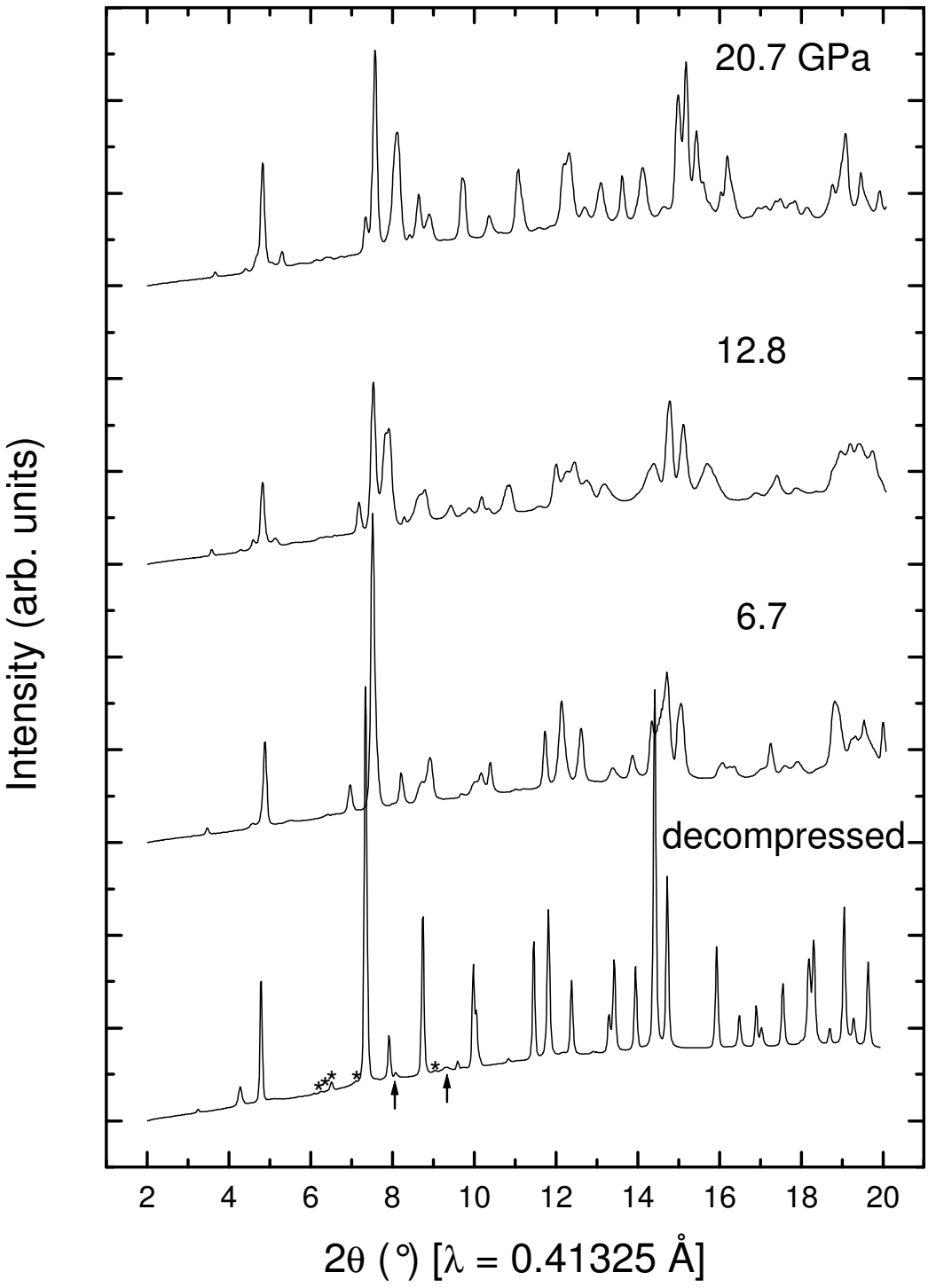
20.7 GPa
12.8
6.7
decompressed
Intensity (arb. units)
2
4
6
8
10
12
14
16
18
20
2θ (°) [λ = 0.41325 Å]

Figure 3.

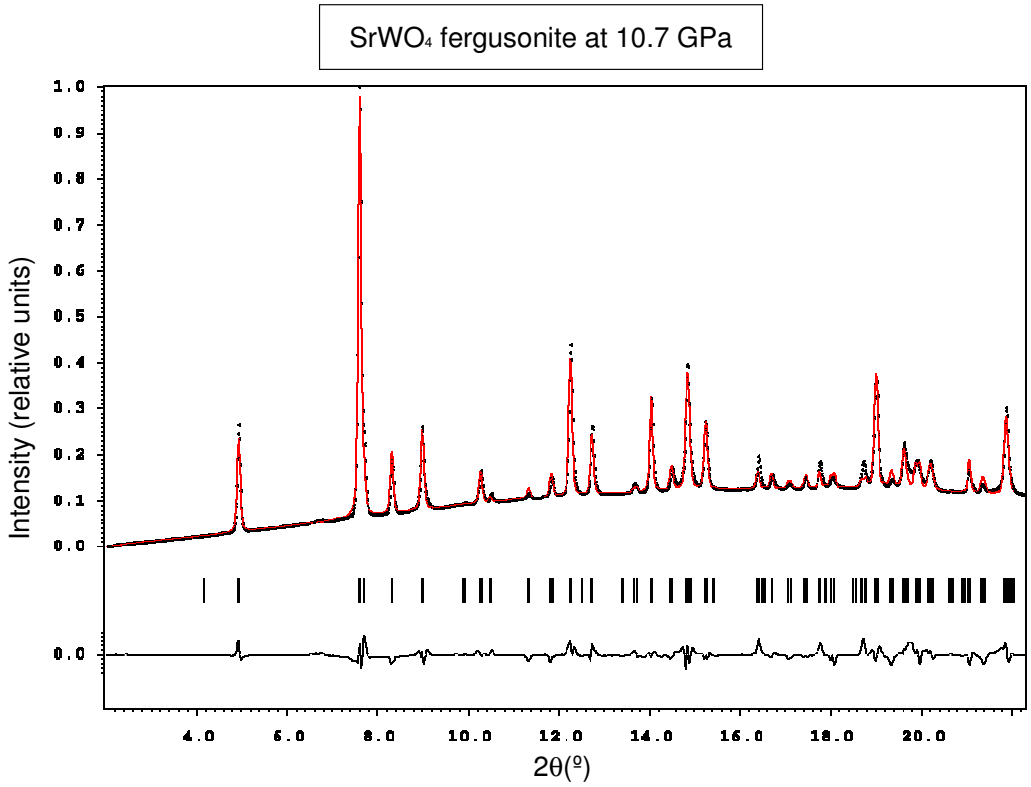
SrWO4 fergusonite at 10.7 GPa
Intensity (relative units)
1.0
0.9
0.8
0.7
0.6
0.5
0.4
0.3
0.2
0.1
0.0
0.0
4.0
6.0
8.0
10.0
12.0
14.0
16.0
18.0
20.0
2θ(º)

Figure 4.

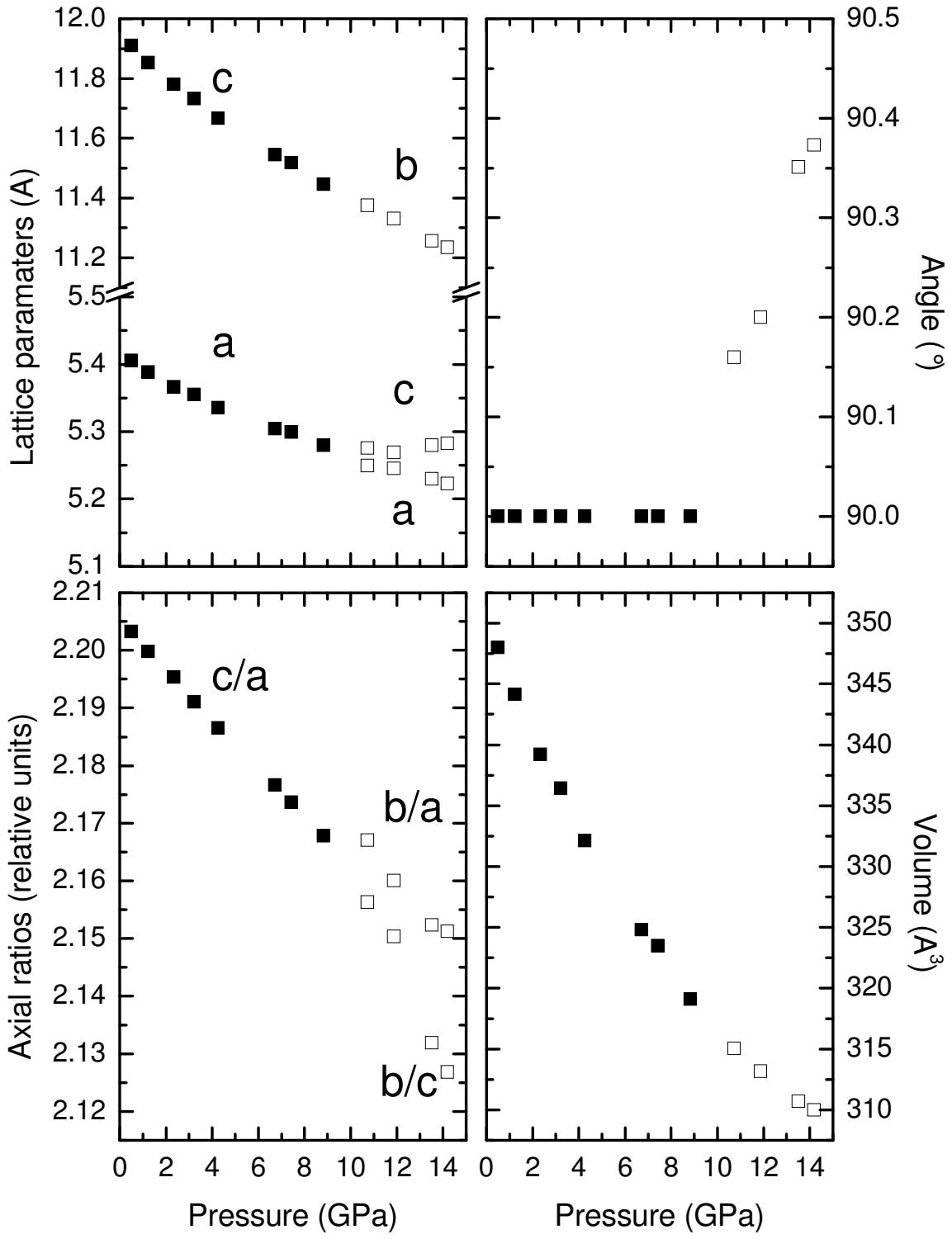
Lattice paramaters (A)
12.0
11.8
11.6
11.4
11.2
5.5
5.4
5.3
5.2
5.1
c
b
a
c
a
Angle (°)
90.5
90.4
90.3
90.2
90.1
90.0
Axial ratios (relative units)
2.21
2.20
2.19
2.18
2.17
2.16
2.15
2.14
2.13
2.12
c/a
b/a
b/c
Volume (A3)
350
345
340
335
330
325
320
315
310
0 2 4 6 8 10 12 14
Pressure (GPa)
0 2 4 6 8 10 12 14
Pressure (GPa)

Figure 5